2015 IEEE/RSJ International Conference on Intelligent Robots and Systems (IROS)
Congress Center Hamburg
Sept 28 - Oct 2, 2015. Hamburg, Germany

Momentum-Driven Single-Actuated Swimming Robot*

Gilad Refael, *Student Member, IEEE* and Amir Degani, *Member, IEEE*

***Abstract*— This paper investigates a simple swimming mechanism, which comprises two concentric bodies and two passive flaps. The mechanism propels itself forward by oscillating its inner body in a symmetric fashion using a single actuator.**

The paper starts by using a simple model to investigate the dynamics of the robot and to simulate its motion. Next, we simulate various design parameters and conclude that some parameters can improve the performance of the swimming robot. We conclude with a proof-of-concept prototype that is capable of swimming similar to the predicted model. Moreover, by using an asymmetric input, the mechanism is able to rotate in various curvatures. The combination of these forward and rotational gaits can be used to stabilize the robot onto a desired trajectory.

I. Introduction and Related Work

We aim to design a swarm of underwater robotic sensors. These mechanisms need not be very fast but should be able to locomote and slowly change formations. We begin by searching for a simple, single-actuated platform that can be idle and static for a long time and can also propel itself. In this current work, we present the first step of design for the planar version of this mechanism. The mechanism uses a single actuator connecting two bodies. By rotating the inner body clockwise, the other rotates counter-clockwise due to the conservation of angular momentum between the two bodies. Alternating the direction of rotation of the inner mass would cause alternating angular velocities of the outer mass. We add two passive flaps to the outer body which open on alternating rotations and effectively cause the desired "swimming" motion of the mechanism as depicted in Fig. 1. For a better understanding of the motion, see the accompanying video. With this conceptual design, the electronics, power, and actuating components can be sealed inside the inner body without any interfacing with the water.

The underlying motivation for this research is that typical autonomous underwater vehicles (AUVs) are, in general, too large, too expensive and in most cases, too complex with numerous actuators and sensors. For example, the REMUS 100 AUV (Kongsberg Maritime, Norway), the Bluefin family of AUVs (Bluefin Robotics, USA) or the MUN explorer [1]. The REMUS 100 AUV is a six degrees-of- freedom AUV packed with sensors and mapping capabilities. It is capable of diving to a 100m depth and is mainly used for hydrographic surveys, military operations, harbor security and oceanic research. It is 160 cm in length and is actually considered a relatively small AUV and costs about $250K. The MUN Explorer AUV is a larger scale AUV capable of deep underwater missions (up to 5000m) and is also fitted with various sensors and imaging equipment. These AUVs are too large and expensive and do not meet our criteria of minimalistic, low cost robots to be used as agents in a robotic swarm.

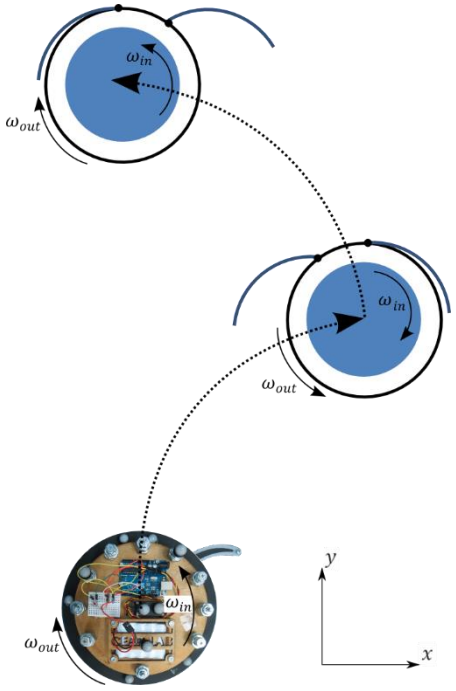

Fig. 1. Typical full cycle of "swimming" motion.

On the other hand, there are projects such as the Autonomous Underwater Explorer [2], a type of robotic "planktonic community" which is used, for example, to sense ocean circulation. Similar to our approach, these sensors are simple, however, and we envision higher maneuverability. Mazumdar and Asada designed an appendage-free, spherical robot [3] which might be used for nuclear inspection of port security. This mechanism might be highly maneuverable, however it loses its simplicity for designing a swarm of simple sensors.

The most common design for underwater robots are from the bio-inspired family, such as eels and fish robots. These mechanisms aim to be both efficient and maneuverable. The eel-like robot, the Amphibot [4], for example, is a modular anguilliform, hyper-redundant swimming robot. Highly impressive robotic fish, such as the MIT's soft robot fish [5], and Essex's robotic fish [6] are examples of bio-inspired

Research supported by Technion - Center for Security Science and Technology (CSST).

G. Refael and A. Degani are with the Technion – Israel Institute of Technology (e-mail: adegani@technion.ac.il).

underwater robots, albeit complex in most cases. Moreover, the robot described here resembles the single-actuated robotic climber [7]. The robotic climber, unlike the one presented here terminates each phase of the cycle by impacting a wall, while our swimming robot does not have a discontinuity but instead gradually changes the drag force between the flap and the surrounding water.

II. Mechanism Concept and Typical Motion

The robot (Fig. 2) comprises two concentric cylindrical bodies connected by a servo which controls the relative angle between them. Two passive flaps are connected to the outer body with their angle of rotation mechanically limited. Due to the conservation of angular momentum, rotating the inner mass will cause the outer unit to rotate in the opposite direction. Alternating the direction of rotation of the inner mass would cause alternating angular velocities of the outer mass. This will cause the desired "swimming" motion of the mechanism as depicted in Fig 1. Each time the motor rotates in one direction, the drag on the flaps causes one of them to open and the opposing one to close. The drag on the open flap creates drag in the positive y-direction while the drag on the closed flap is smaller, causing the body to move forward.

III. Dynamical Model

In experiments, our system showed a swimming behavior similar to our hypothesis in Sec. II. The goal of this section is to produce a simple model that exhibits a similar behavior to our mechanism. In our simplified model, the mechanism is planar and consists of two concentric bodies. The sole control of the robot is the relative angle ϕ between the two bodies. We define the configuration of the robot to be $q = (x, y, \theta_{in}, \theta_{out})^T$, where x, y are the coordinates of the robot's center and $\theta_{in}, \theta_{out}$ are the orientations of the inner and outer bodies, respectively, as shown in Fig. 2 (right). The relative angle, ϕ, between the two bodies is a kinematic constraint and is chosen as a symmetric sinusoidal input ($\phi(t) = A \sin \omega t$). In the first half cycle, seen in Fig. 1, as the inner body rotates counter-clockwise, the outer body rotates clockwise and the right flap opens. We assume the transient flap opening time is negligible. Since the flap open angle, ψ, is mechanically limited, the body and the currently open flap are assumed to be one rigid body. Finally, the relative velocity between the water and the flap v_{flap} does not change along the flap. This means that the lift force is acting in the middle of the flap length. We will validate these assumptions in experiments in Sec. V.

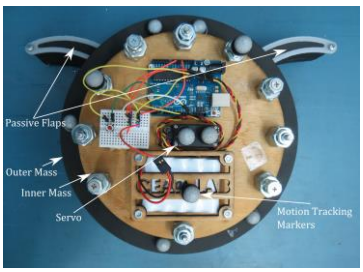

(a)

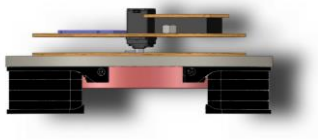

(b)

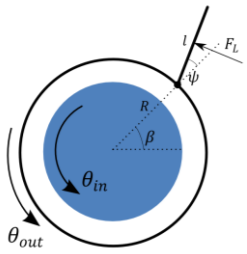

(c)

Fig. 2. (a) top and (b) side view of proof-of-concept mechanism. (c) Model notation and definitions. The notations θ_{in} and θ_{out} represent the positive directions, although due to the conservation of angular momentum, the angles are typically in opposite directions.

To produce the equations of motion, we define the Lagrangian as

$$\mathcal{L} = \frac{1}{2} I_{in} \dot{\theta}^2{}_{in} + \frac{1}{2} I_{out} \dot{\theta}^2{}_{out} + \frac{1}{2} m(\dot{x}^2 + \dot{y}^2), \qquad (1)$$

where I_{in}, I_{out} are the moments of inertia of the inner and outer parts respectively, and m is the total mass of the robot. All system's parameters definition used in the following section are shown in Table I.

Since the outer body is connected to the inner body by a servo motor, we assume that the servo motor satisfies the constraint $\theta_{in} = \theta_{out} + \phi$. Hence, the configuration vector can be reduced to $q = (x, y, \theta)^T$ where $\theta := \theta_{out}$.

For a single half-cycle, the lift force F_L acting perpendicular to the (currently open) flap and the drag force F_D acting on the outer mass (Fig. 2) are calculated from the forces acting on a differential area dA of the flap and outer body

$$\begin{aligned} dF_L &= \frac{1}{2} \rho c_L v_{flap}^2 dA_{flap} \\ dF_D &= \tfrac{1}{2} \rho c_D v_{out}^2 dA_{out}. \end{aligned} \qquad (2)$$

Integrating (2) over the flap and outer body respectively yields

$$\begin{aligned} F_L &= \alpha_L \dot{\theta}^2 \\ F_D &= \alpha_D (\dot{x}^2 + \dot{y}^2) \\ M &= F_L (R \cos\psi + r_f), \end{aligned} \qquad (3)$$

where, $\alpha_L = \frac{1}{2} \rho c_L b l \left(R + \frac{l}{2}\right)^2$, $\alpha_D = \frac{1}{2} \rho c_D \pi R h_{wet}$.

Using Lagrange's equations on (1) and inserting the generalized forces (3), yields the equations of motion in the robot's reference frame

$$\begin{aligned} m\ddot{x} = &-\frac{1}{2} \rho c_L b L \left(R + \frac{L}{2}\right)^2 sin(\beta + \psi)\, \dot{\theta}^2 \\ &-\frac{1}{2} \rho c_D \pi R h_{wet} (\dot{x}^2 + \dot{y}^2)^{\frac{1}{2}} \dot{x} \end{aligned} \qquad (4)$$

$$\begin{aligned} m\ddot{y} = &\frac{1}{2} \rho c_L b L \left(R + \frac{L}{2}\right)^2 cos(\beta + \psi)\, \dot{\theta}^2 \\ &-\frac{1}{2} \rho c_D \pi R h_{wet} (\dot{x}^2 + \dot{y}^2)^{\frac{1}{2}} \dot{y} \end{aligned} \qquad (5)$$

$$\begin{aligned} &(I_{in} + I_{out})\ddot{\theta} + I_{in}\ddot{\phi} = \\ &\quad \tfrac{1}{2} \rho c_L b L \left(R + \tfrac{L}{2}\right)^2 (R\, cos\, \psi + r_f) \dot{\theta}^2. \end{aligned} \qquad (6)$$

We further non-dimensionalize (4)-(6) using a characteristic time of $1/\omega$ and characteristic length of l (the

length of the flap) to achieve the new set of non-dimensional equations of motion:

$$\ddot{x} = -c_1 \sin(\beta + \psi)\,\dot{\theta}^2 \tag{7}$$

$$\ddot{y} = c_1 \cos\,(\beta + \psi)\,\dot{\theta}^2 \tag{8}$$

$$\ddot{\theta} + I\ddot{\phi} = c_2\dot{\theta}^2 \tag{9}$$

where,

$$c_1 = \frac{1}{8m}\rho c_L b(2R + L)^2$$

$$c_2 = \frac{1}{8(I_{in}+I_{out})}\rho c_L bL(2R + L)^2(R\cos\psi + r_f).$$

Lastly, we transform these equations to the world coordinates with a rotation matrix $R(\hat{z}, \theta_{out})$.

The non-dimensional coefficients c_1 and c_2 represent the ratio between the drag and inertial forces and moments, respectively, and I is the non-dimensional moment of inertia ratio. A large value of I means that the outer body will rotate more, or in other words, the input ϕ will have a larger influence on θ and will cause a larger angular acceleration, hence, causing a faster forward motion.

It can be seen in (6) and (7) that the differential equation is invariant to the orientation θ. Therefore, a perturbation in θ will not grow nor decay which means we can already expect the system to be marginally stable.

IV. Simulations

In this section we perform simulations of the dynamic model described in Sec. III with the purpose of validating the model. We first simulate a typical swimming motion (Fig. 3). Furthermore, we then use the simulation to sweep through different values of the system's parameters (Fig. 4) and to get insight on what effect some parameters have on the dynamics of the system, e.g., forward velocity, which might be harder to change in experiment.

The simulations were performed in MATLAB™ ode23s solver with a relative tolerance of 10^{-4} and an absolute tolerance of 10^{-6}. Unless mentioned otherwise, we use the parameter values from Table I.

TABLE I.
PARAMETERS FOR MODELING AND SIMULATION SECTIONS

Dimensional Parameters		
Parameter	***Description***	***Value***
m	*total mass*	$1.03\ kg$
b	*flap height*	$0.044\ m$
L	*flap length*	$0.09\ m$
R	*outer mass radius*	$0.08\ m$
ρ	*water density*	$1000\ kg/m^3$
h_{wet}	*wet height*	$0.35\ m$
Non-dimensional (ND) Parameters		
Parameter	***Description***	***Value***
I	*ND moment of inertia* $\frac{I_{in}}{I_{in}+I_{out}}$	0.7421
β	*flap location*	30°
ψ	*flap open angle*	20°
c_L, c_D	*lift and drag coefficients*	
c_1	*linear drag-inertia ratio*	
c_2	*angular drag-inertia ratio*	

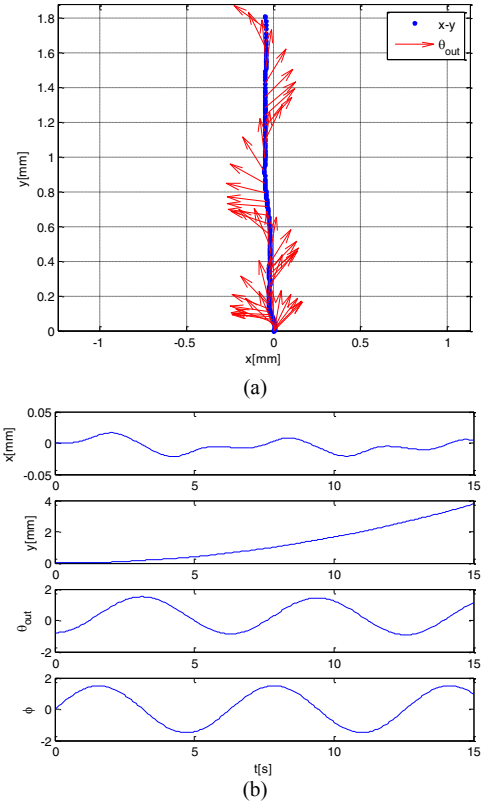

(a)

(b)

Fig. 3 Symmetric input ($\phi(t) = A\sin\omega t$). (a) x vs. y, and (b) configuration plot. The numeric solution was sensitive to calculation errors which corresponds with the marginal stability of the system.

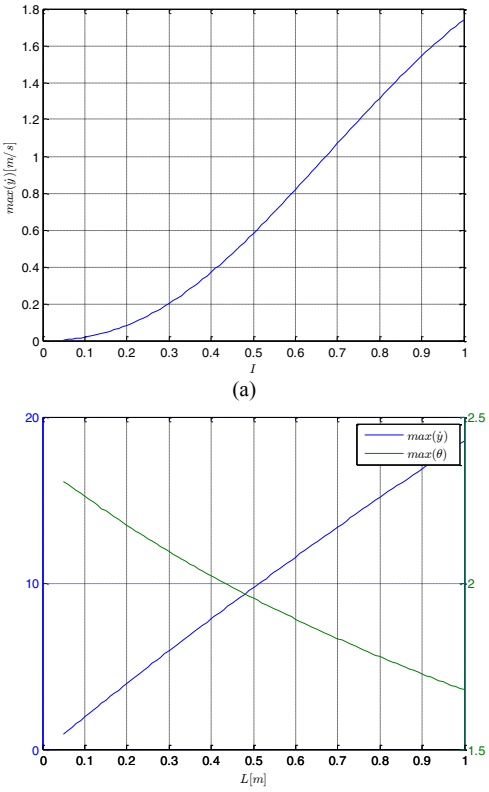

(a)

(b)

Fig. 4 Parameter sweep. (a) maximal forward velocity vs. I, (b) maximal forward velocity and angle vs. flap length L.

The model was modified to account for the whole cycle of motion using the sign function, i.e., switching the equations of motion according to the currently open flap.

The results of the first simulation with a symmetric input, i.e. $\phi(t) = A\sin\omega t$, are shown in Fig. 3. The x, y coordinates of the robot are shown in blue and the orientation in red arrows. We can see a monotonic forward motion in y, along with small oscillations in x. With the present model, the simulation can only accurately simulate a motion using a symmetric input.

We ran a parameter sweep of two of the parameters: the non-dimensional moment of inertia I (Fig.4.a) and the flap length L from 0.05 to 1 (Fig.4.b). As expected, increasing I ($I = 1 \leftrightarrow I_{out}/I_{in} = 0$) creates a greater effect of the input on the system and yields an increased amplitude of the orientation θ, hence, faster forward motion. Increasing the flap length, L, creates a similar response in terms of the forward motion along with a reduced amplitude of the orientation θ.

V. Experiments

In this section, we describe the mechanical design, the experimental setup, and experiments with different inputs. We begin by experimentally checking the validity of the assumptions from Sec III. For additional videos of experiments in a similar setup, see accompanying video.

A. Experimental Setup

The proof-of-concept mechanism (shown in Fig. 2) was built from 3D printed and laser cut parts. It is controlled by an Arduino Uno and powered by a 6V battery pack. The servo (Hitec HS5645-MG) provides a torque up to 12.1 kg/cm at 0.18 sec/60°. We have placed reflective markers on both of the robot's bodies to track their motion. The nuts along the edge of the inner mass were added to increase I_{in} and increase the rotation of the outer mass. The experiments were ran in an open-loop, preprogrammed input ϕ.

The experimental setup comprises a small swimming pool and the Vicon T10S motion capture system (Vicon Motion Systems, Ltd., UK). Six Vicon cameras are located above the pool providing position and orientation tracking at 1000 Hz frame rate and 2 mm accuracy. The measurements were projected onto the pool's plane since the out-of-plane motions were neglected.

B. Dynamic Model Validation

In Sec III, we used a few assumptions to allow a simplified dynamic model. We ran several experiments which validate these assumptions.

Kinematic Constraint (ϕ): We tracked the relative angle between the inner and outer bodies while inputting a symmetric ϕ constraint. In all experiments the fit was nearly perfect to a sinusoidal wave (R=0.996).

Validate Flap Open Time: in the experiments the transient flap opening time is approximately 130 msec, while the fully open time of the flap is approximately 400 msec. With a symmetric input, this un-modeled delay affects both half-cycles in a similar manner therefore do not expect to have a significant impact on the simulation results.

C. Symmetric Input ϕ

The first experiment we conducted (Fig. 5) uses a symmetric angular constraint between the two bodies, i.e., $\phi(t) = A\sin\omega t$.

Fig. 5.a shows the x, y position in blue and orientation of the outer body (θ_{out}) in red arrows. Fig. 5.b shows the angular

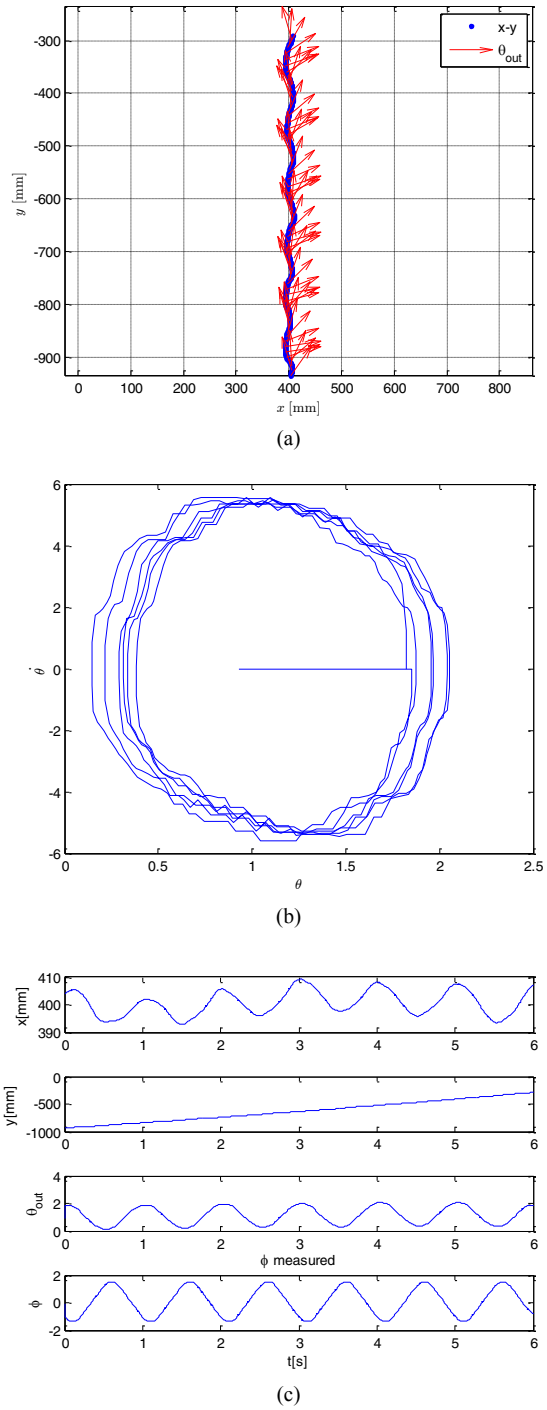

Fig. 5. Symmetric input ($\phi = A\sin\omega t$). (a) x vs. y, (b) phase plot, (c) configuration plot. It can be seen that mechanism indeed is being propelled in the y-direction, however it does not seem to be stable as seen in (a) and (b).

phase plot (θ vs. $\dot{\theta}$), and finally the Fig. 5.c shows the robot's configurations vs. time $(x(t), y(t), \theta(t), \phi(t))$. As can be seen, the forward propulsion is monotonic; phase plot shows a marginally stable system, however as can be seen in the bottom figure, toward the end of the experiment the system begins to diverge.

As discussed in Sec. III, the fact that the system is marginally stable is not surprising and could have been deduced by observing (9), i.e., that the differential equation is invariant to the orientation θ.

D. *Asymmetric Input ϕ*

As we saw in the previous experiment, a perturbation in the system will not converge back, and is hence not stable. In order to force the system back on path, we tried to find a way to "steer" the mechanism.

We found that a rotation can be achieved using an asymmetric input, i.e., a sinusoidal input with a different frequency for each half period. For a single period, the input is

$$\phi(t) = \begin{cases} A \sin \omega_1 t & t \in \left[0, \frac{T_1}{2}\right] \\ A \sin \omega_2 \left(t - \frac{1}{2}(T_1 + T_2)\right) & t \in \left[\frac{T_1}{2}, \frac{T_1 + T_2}{2}\right] \end{cases} \quad (10)$$

where T_1, T_2 are the periods of ω_1, ω_2, respectivly. For t outside $\left[0, \frac{T_1+T_2}{2}\right]$ we use the modulus operator $t \; mod \left(\frac{T_1+T_2}{2}\right)$. Experimental results of this steering motion are shown in Fig. 6.

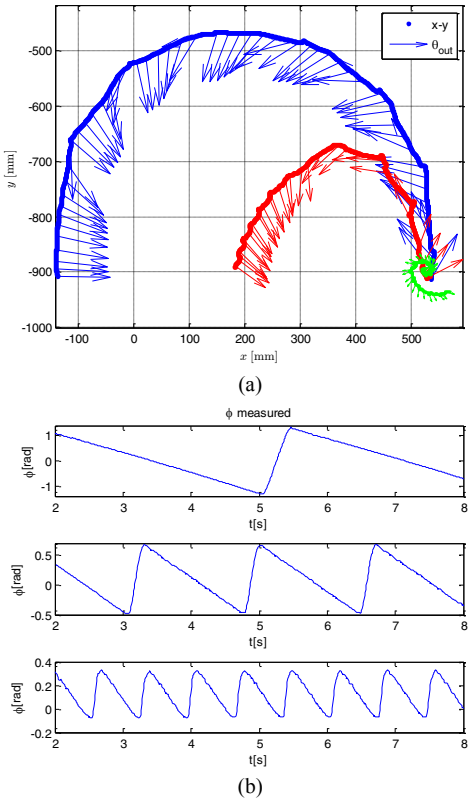

Fig. 6. Experiments with asymmetric input ϕ. (a) x vs. y plot showing three different input parameters. (b) the three asymmetric inputs. Top slow input causes a relatively large turning radius, while bottom fast input causes a tight turning radius.

E. *Combining symmetric and asymmetric input*

As a preliminary experiment regarding control and motion planning of the robot, we performed an open-loop experiment involving its primitive motions i.e., forward motion and rotation. The goal was to swim forward, rotate 180° and swim the same distance back. Results of this combined motion can be seen in Fig. 7.

VI. Conclusion and Future Work

The larger goal of this research is to design a swarm of underwater robotic sensors which are idle most of the time and have the ability to occasionally maneuver. These maneuvers can be used to better sense an intruder in a port, detect a plume, or to perform a swarm reformation. These mechanisms need not be very fast but should be able to locomote and stay cheap and simple. In this paper we discussed the mechanism design principle of articulating an inner-body in order to counter rotate the outer-body. By attaching passive flaps to the outer-body that open only when rotated in a specific direction, the mechanism rocks back and forth and achieves a net forward propulsion. We simplified the model, derived the dynamic equations of motion and performed numerical simulations checking a few crucial design parameters. We have found that increasing the moment of inertia ratio I closer to 1, the net angular velocity gets closer to the input ϕ. Moreover, by making the flap longer we get faster "forward" motion with

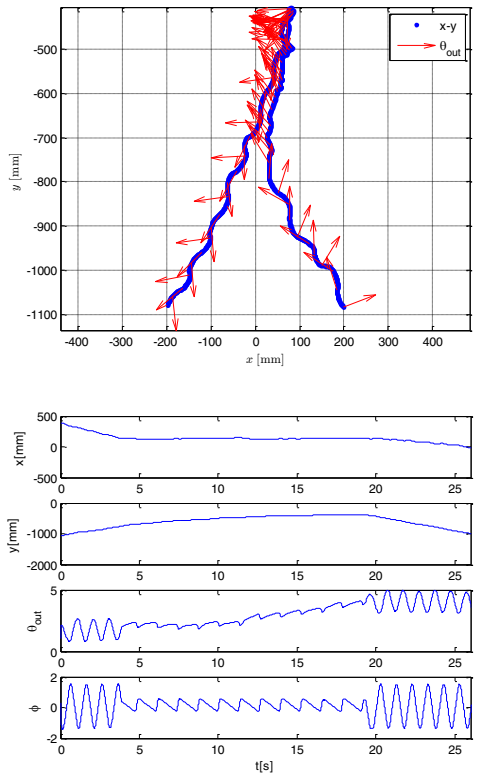

Fig. 7. Combining symmetric and asymmetric input. The system propels forward for 3.4 seconds, then rotates in its place 180º, then once again propels forward.

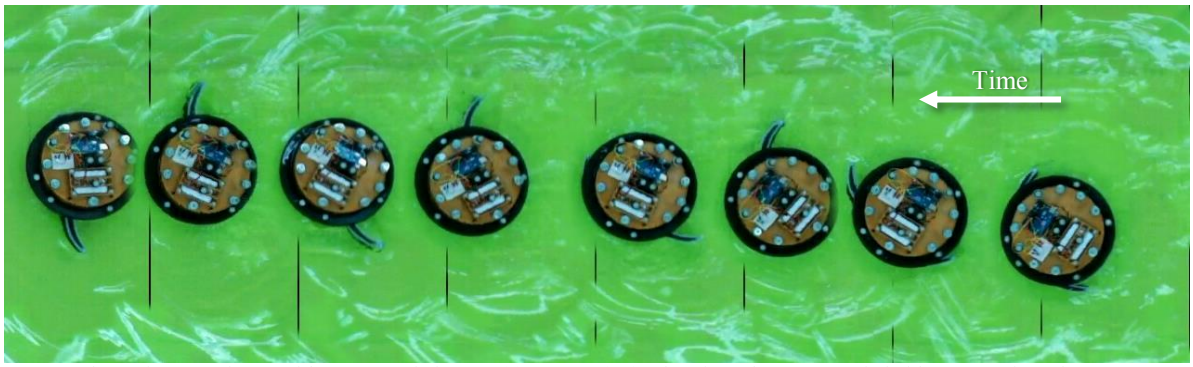

Fig. 8. Snapshots of an experiment with a symmetric input $\phi(t) = A\,sin(\omega t)$ taken from the accompanied video, approximately 500 msec apart.

less lateral motion. We have also conducted a number of experiments with our proof-of-concept mechanism and showed the difference in the motion when using a symmetric versus asymmetric input by showing that an asymmetric input causes the mechanism to rotate. By using different asymmetries, we are able to achieve different turning radii. This will be key to closing the loop and to enable the mechanism to follow desired trajectories.

In future work, we plan to improve the model of the robot by including the flaps' dynamics, i.e., solving a three-body dynamical system. The improved model will take into account the open and close time of the flaps which will allow us to relax the assumptions and hopefully simulate the asymmetric motion as well. We also intend to sense the average orientation and perform motion planning using the primitive motions described in this current work. We intend to insert a spring in series to the actuator between the two bodies to create a series elastic actuator. We believe this will enable stable swimming and might also increase the efficiency.

We will also continue to work toward our ultimate goal, a 3-D underwater submersible maneuverable sensor. In order to do so, we will include another pair of passive flaps, or include a pressurized ballast to control the depth and use a similar planar mechanism for in-plane maneuvers.

ACKNOWLEDGMENT

The authors wish to thank Alon Danay for helping in prototyping and experiments, and Andy Ruina and Uri Shavit for helpful suggestions.

REFERENCES

[1] M. T. Isaac, S. Adams, M. He, N. Bose, C. D. Williams, R. Bachmayer and T. Crees, "Manoeuvring experiments using the MUN Explorer AUV," in *Underwater Technology and Workshop on Scientific Use of Submarine Cables and Related Technologies*, 2007.

[2] R. Kastner, A. Lin, C. Schurgers, J. Jaffe, P. Franks and B. S. Stewart, "Sensor platforms for multimodal underwater monitoring," in *in 2012 International Green Computing Conference (IGCC)*, 2012.

[3] A. Mazumda and H. Asada, "Control-Configured Design of Spheroidal, Appendage-Free, Underwater Vehicles," *IEEE Transactions on Robotics,* vol. 30, no. 2, pp. 448-460, April 2014.

[4] A. Crespi and A. J. Ijspeert, "AmphiBot II: An amphibious snake robot that crawls and swims using a central pattern generator," in *In Proceedings of the 9th international conference on climbing and walking robots (CLAWAR 2006)*, 2006.

[5] A. D. Marchese, C. D. Onal and D. Rus, "Autonomous soft robotic fish capable of escape maneuvers using fluidic elastomer actuators," *Soft Robotics,* vol. 1, no. 1, pp. 75-87, 2014.

[6] J. Liu and H. Hu, "Biological inspiration: from carangiform fish to multi-joint robotic fish," *Journal of Bionic Engineering,* vol. 7, no. 1, pp. 35-48, 2010.

[7] A. Degani, H. Choset and M. T. Mason, "DSAC-Dynamic, single actuated climber: local stability and bifurcations," in *Robotics and Automation (ICRA), 2010 IEEE International Conference on,*, 2010.